Cross Correlate Tidal Reconstructed 21cm Signal with Kinematic Sunyaev-Zel'dovich Effect: A New Probe for Missing Baryons at $z \sim 1-2$

We propose a new way to study baryon abundance and distribution at mid redshift. We cross correlate density field from HI 21cm intensity mapping with temperature anisotropy of Cosmic Microwave Background(CMB) caused by raidal motion of free electrons, i.e. kinetic Sunyaev-Zel'dovich (kSZ) effect. We put forward a 3D cosmic tidal reconstruction to recover the modes lost in 21cm foregrounds, which will effectively promote the apprearance of correlation signals.

We verify the idea with simulation outputs on $z = 1, z = 2$, taking into account of foreground noises, facility resolutions, and redshift distortions. We successfully recover $> 90\%$ information of the 21cm density field at $k \sim 0.01h/Mpc$ after tidal reconstruction. We obtain a $r > 0.6$ correlation with origin kSZ signal from $l \sim 100 - 2000$. Assuming the noise level of Planck, there will be $\sim 3 - 20\sigma$ signal from $l \sim 300 - 4000$ for $z \sim 1$, $\sim 3 - 40\sigma$ signal from $l \sim 300 - 5000$ for $z \sim 2$.

This is a very promissing probe to study diffused matter distribution. 1. It is less biased towards local density contraction, thanks to the kinetic nature of kSZ signals; 2. It has precise redshift information from 21cm spectrum; 3. It is rather feasible to get required data of higher redshifts with large sky coverage. The 21cm intensity mapping survey has huge advantage on survey speed, facility requirements and costs comparing to spectrocscopic galaxy survey.

Consider the simulated S/N level, data requirements, current and upcoming 21cm intensity mapping facilities, we are optimistic about the new probe.

PACS numbers:

I. INTRODUCTION

While the baryon abundance of early universe is well fixed by the cosmic microwave background (CMB),Big Bang Nucleosynthesis and Lyman-α forest [1][2][3][4], a deficiency was noiticed in local universe. At $z \lesssim 2$ the detected baryon content in collapsed objects, eg. galaxies, galaxy clusters and groups, only account for 10% of the predicted amount. More baryons are believe to reside in Warm-Hot Intergalactic Mediums (WHIM) with typical temperature of 10^5 K to 10^7 K [5], which is too cold and diffuse to be easily detected. Continuous effort has been made to detect this part of the baryons. One common approach is using hydrogen and metal absorption lines(eg, HI, Mg II,Si II, C II, Si III, C III, Si IV, O VI, O VII) [6][7]. However, the lines are usually limited to close circumgalactic medium, while at least 25% of the baryons are bebieved to reside in more diffused region [8]. Moreover, the uncertainty in metalicity would sometimes reduce the reliability.

A promising tool to probe the missing baryon is the kinetic Sunyaev-Zel'dovich(kSZ) effect [9][10], an effect that is known for its great potential to explore the Epoch of Reionization. It refers to the secondary temperature anisotropy in CMB caused by radial motions of free electrons, which only correlates to electron density and velocity, regardless the temperature and pressure. Since the velocity field mainly results from large scale structure, the method is less biased towards hot, compact place, and provide more information on the fraction of diffused baryons.

Attractive as it is, due to the contamination from primary CMB and residual thermal SZ signal it is difficult to filter the kSZ signal without other sources. Worse still, the signal itself does not contain redshift information.

To fix this, previous approches cross correlated it with galaxy surveys, eg. using pairwise-momentum estimator [11] or velocity-field-reconstruction estimator [12][13]. However since they all require spectroscopy of galaxies to provide accurate redshift, the sky volume and redshift range to apply the method is limited. A recent effort try to fix this by using photometries of infrared-selected galaxies. However, since they used projected fields of the galaxies, they could only obtain a rough estimate over a wide redshift bin [14].

In this paper we present a new cross relating source, HI density field, from 21cm intensity mapping, a kind of surveys that provide integrated signals of diffuse 21cm spectra, rather than detecting individual objects.

It will make it feasible to probe the baryon content to $z \gtrsim 1$ in very near future, with ongoing experiments like CHIME [15], Tianlai [16], HIRAX [17] etc. . Besides, the 21cm spectrum contains accurate redshift information, which makes it a good candidate to be cross correlated to kSZ signals.

This powerful probe was rarely harnessed in this topic previously, because the continuum foregrounds in 21cm measurements is typically 10^2-10^3 times brighter than cosmological signals, almost completely bury the distribution of large scale structures in radial direction, i.e. modes with small $k_\parallel$. Meanwhile the veocity field is closely related with the large scale structure, which makes the correlation difficult to see.

To compensate that, a new method called *cosmic tidal reconstruction* has been developed recently [18][19]. It can reconstruct the large scale density field from the alignment of small scale cosmic structures. In this paper, we further extend the previous 2D tidal reconstruction to 3D–this is a necessity since we need more accurate large scale density field on z directions. We discuss the influence of redshift distortions for that.

Applying this methods to foreground substracted 21cm density fields, we obtain a sufficiently good cross-correlation signal with original kSZ signals.

The paper is organized as follows. In section II, we present the complete procedure: II A, Introduce 3D tidal reconstruction method; II B, How to use reconstructed fields to cross

correlate with kSZ signals; In section III, we present the simulations: III A, Simulation set up; III B, Simulations results; In section IV, we discuss the error and demonstrate the importance of tidal reconstruction: IV A, Redshift distortion; IV B, Statistical error; IV C, non-tidal reconstructed cross correlation; In section V, we give conclusions and discuss future applications.

II. COMPLETE PROCEDURE AND SIMULATION RESULTS

A. 3D Cosmic Tidal Reconstruction

While a cosmic signal in 21cm measurement is of the order of mK, foregrounds coming from Galactic emissions, telescope noise, extragalactic radio sources and Radio recombination lines, can reach the order of Kelvin [20][21]. Lots of techniques have been developed to substract the foregrounds, taking advantage of the attribute that they have fewer bright spectral degrees of freedom[22]. Unfortunately, the substraction usually contaminates the smooth large scale structure information. Since the large scale information is essential for the estimate of peculiar velocity, we need to recover the information. iHowever, since large scale structure is correlated closely to the emergence of peculiar velocity, we need a method to estimate its distribution.

The cosmic tidal reconstruction is a kind of quadratic statistics developed to achieve this goal. Its main idea is using small scale filamentary structures to solve for the large scale tidal shear and gravitational potential.

Here, we present a 3 dimentional reconstruction algorithm that works best in close linear regions.

First, we filter for the small scale structures that are most likely to be influenced by tidal force of large scale fields.

(1) Convolve the field with a Gaussian kernal $S(\boldsymbol{k}) = e^{-k^2R^2/2}$, we take $R = 1.25\ \mathrm{Mpc}/h$ [18], to reduce the complicated non-linear effects on small scales.

(2) Gaussianize the field, by taking $\delta_g = \ln(1+\delta)$. This is to allieviate the problem that filter W_i in (3) heavily weights high density regions.

(3) Apply filter $W_i(\boldsymbol{k})$, which assigns weights to δ_g according to predicted displacements caused by tidal field in near linear regions [19]. $\delta_g^{w_i}(\boldsymbol{k}) = W_i(\boldsymbol{k})\delta_g(\boldsymbol{k})$,

$$W_i(\boldsymbol{k}) = (\frac{P(k)f(k)}{P_{tot}^2(k)})^{\frac{1}{2}}\hat{k}_i \tag{1}$$

i indicates $\hat{x}, \hat{y}, \hat{z}$ directions, $P_{tot} = P + P_{noise}$ is observed matter powerspectrum, P is theoretical matter powerspectrum, $f = 2\alpha(\tau) - \beta(\tau) dlnP/dlnk$, where α and β are functions related to linear growth funcion, and are calculated to be (0.6, 1.3) for $z = 1$ and (0.4, 0.9) for $z = 2$. [1]

[1] The effect of the filter W_i on different scales could be seen in Appendix 1.

Second, we estimate the tidal force and hense reconstruct the large scale density field.

(1) Following gravitational lensing procedures, we decompose the 3×3 symmetric, traceless tidal force tensor into 5 γ components, and estimate them from density variance.

$$\begin{aligned}
\hat{\gamma}_1(\boldsymbol{x}) &= [\delta_g^{w_1}(\boldsymbol{x})\delta_g^{w_1}(\boldsymbol{x}) - \delta_g^{w_2}(\boldsymbol{x})\delta_g^{w_2}(\boldsymbol{x})],\\
\hat{\gamma}_2(\boldsymbol{x}) &= [2\delta_g^{w_1}(\boldsymbol{x})\delta_g^{w_2}(\boldsymbol{x})],\\
\hat{\gamma}_x(\boldsymbol{x}) &= [2\delta_g^{w_1}(\boldsymbol{x})\delta_g^{w_3}(\boldsymbol{x})],\\
\hat{\gamma}_y(\boldsymbol{x}) &= [2\delta_g^{w_2}(\boldsymbol{x})\delta_g^{w_3}(\boldsymbol{x})],\\
\hat{\gamma}_z(\boldsymbol{x}) &= [(2\delta_g^{w_3}(\boldsymbol{x})\delta_g^{w_3}(\boldsymbol{x}) - \delta_g^{w_1}(\boldsymbol{x})\delta_g^{w_1}(\boldsymbol{x}) - \delta_g^{w_2}(\boldsymbol{x})\delta_g^{w_2}(\boldsymbol{x}))]/3,
\end{aligned} \tag{2}$$

(2) Reconstruct 3D density field.

$$\begin{aligned}
\kappa_{3\mathrm{D}}(\boldsymbol{k}) &= \frac{1}{k_1^2+k_2^2+k_3^2}[(k_1^2-k_2^2)\gamma_1(\boldsymbol{k}) + 2k_1k_2\gamma_2(\boldsymbol{k})\\
&\quad +2k_1k_3\gamma_x(\boldsymbol{k}) + 2k_2k_3\gamma_y(\boldsymbol{k}) + (2k_3^2-k_1^2-k_1^2)\gamma_z(\boldsymbol{k})].
\end{aligned} \tag{3}$$

Third, we correct bias and suppress noise with a Wiener filter. Due to the foregrounds, the noise in z direction will be different from x,y direction, therefore we apply an anisotropic Wiener filter.

$$\hat{\kappa}_c(\boldsymbol{k}) = \frac{\kappa_{3D}(\boldsymbol{k})}{b(k_\perp, k_\parallel)} W(k_\perp, k_\parallel)\ , \tag{4}$$

Bias $b = \frac{P_{k3D\delta}}{P_\delta}$, Wiener filter $W = \frac{P_\delta}{P_{k3D}/b^2}$.

Here and afterwards, we use "$\wedge$" to denote recontructed fields.

B. Velocity Reconstruction and kSZ signals

Due to the cancellation of positive and negative velocity, direct cross correlation between kSZ signal and density field will vanish. Therefore, we first estimate the peculiar velocity from the 3D density field, then construct the 2D map of kSZ signal, finally correlate it with the real kSZ signal [12].

Detailed steps are as follows.

(1) Estimate the velocity field:

In linear region, the continuity equation goes like: $\dot{\delta} + \nabla \cdot \boldsymbol{v} = 0$, where $\boldsymbol{v}$ is the peculiar velocity and δ is the matter overdensity.

Therefore, we obtain an estimator of velocity distribution:

$$\hat{v}_z(\boldsymbol{k}) = iaH\frac{d\ln D}{d\ln a}\delta(\boldsymbol{k})\frac{k_z}{k^2} \tag{5}$$

where D(a) is the linear growth function.

$v_z \propto \frac{k_z}{k^2}$, indicating the most prominent signal comes from small k mode, which corresponds to large scale structure. This further verify our motivation for tidal reconstruction procedure.

(2) suppress the noise in velocity field with a new Wiener filter, following identical procedure as Eq.(4). This is because the term $\frac{k_z}{k^2}$ in Eq.(5) will strongly amplify noises in small k modes.

(3) Calculate 2D kSZ map.

The CMB temperature fluctuations caused by kSZ effect is:

$$\Theta_{kSZ}(\hat{n}) \equiv \frac{\Delta T_{kSZ}}{T_{\rm CMB}} = -\frac{1}{c}\int d\eta g(\eta) \boldsymbol{p}_{\parallel}\,, \tag{6}$$

where $\eta(z)$ is the comoving distance at redshift z, $g(\eta) = e^{-\tau} d\tau/d\eta$ is the visibility function, τ is the optical depth to Thomson scattering, $\boldsymbol{p}_{\parallel} = (1+\delta)\boldsymbol{v}_{\parallel}$, with δ the electron overdensity. We assume that $g(\eta)$ doesn't change significally in one redshift bin, and integrate $\boldsymbol{p}_{\parallel}$ along radial axis to get $\hat{\Theta}_{kSZ}$

(4) Calculate correlation coefficients.

We compare reconstructed kSZ signals $\hat{\Theta}_{kSZ}$ with kSZ signals Θ_{kSZ} directly from simulations. To quantify the tightness of correlation, we employ a quantity r:

$$r \equiv \frac{P_{recon,real}}{\sqrt{P_{recon} P_{real}}} \tag{7}$$

C. Simulation Set up

We use six N-body simulations from the CUBEP^{3}M code [23]. Each evolves 1024^3 particles in a $(1.2{\rm Gpc}/h)^3$ box. with following cosmological parameters: Hubble parameter $h = 0.678$, baryon density $\Omega_b = 0.049$, dark matter density $\Omega_c = 0.259$, amplitude of primordial curvature power spectrum $A_s = 2.139 \times 10^{-9}$ at $k_0 = 0.05$ Mpc^{-1} and scalar spectral index $n_s = 0.968$. We analyse the outputs at both redshift 1 and 2.

For simplicity, we assume the experimental noise to be zero above a cut off scale and infinity below the cut off scale. This is a reasonable approximation for a filled aperture experiment, which has good brightness sensitivity and an exponetially growing noise at small scales. We choose this scale to be $k_c = 0.5\ h/{\rm Mpc}$, which corresponds to $\ell = 1150$ at $z = 1$. This is realistic for the ongoing 21cm experiments like CHIME [15][24] and Tianlai [25][16]. copied

To mimic the influence of foreground substraction, we use a high pass filter $W_{fs}(k_{\parallel}) = 1 - e^{-k_{\parallel}^2 R_{\parallel}^2/2}$. We choose $R_{\parallel} = 15\ {\rm Mpc}/h$, which gives $W_{fs} = 0.5$ at $k_{\parallel} = 0.08\ {\rm Mpc}/h$. This corresponds to the condition of current 21cm observations [26][27].

The observed 21cm field after foreground subtraction is given by

$$\delta_{fs}(\boldsymbol{k}) = \delta(\boldsymbol{k}) W_{fs}(k_{\parallel}) \Theta(k_c - k), \tag{8}$$

where $\delta(\boldsymbol{k})$ is the density field from simulations, W_{fs} accounts for the effect of foreground subtraction and $\Theta(x)$ is the step function which equals 1 for $x \geq 0$ and otherwise 0. Then we get the reconstructed clean field $\hat{\kappa}_c$ from δ_{fs} via cosmic tidal reconstruction. Using $\hat{\kappa}_c$ we obtain an estimate radial velocity field $\hat{v}_z$ as in Eq.(5). And then we reconstruct the kSZ signal following Eq.(6) and compare it with the kSZ signal from simulations.

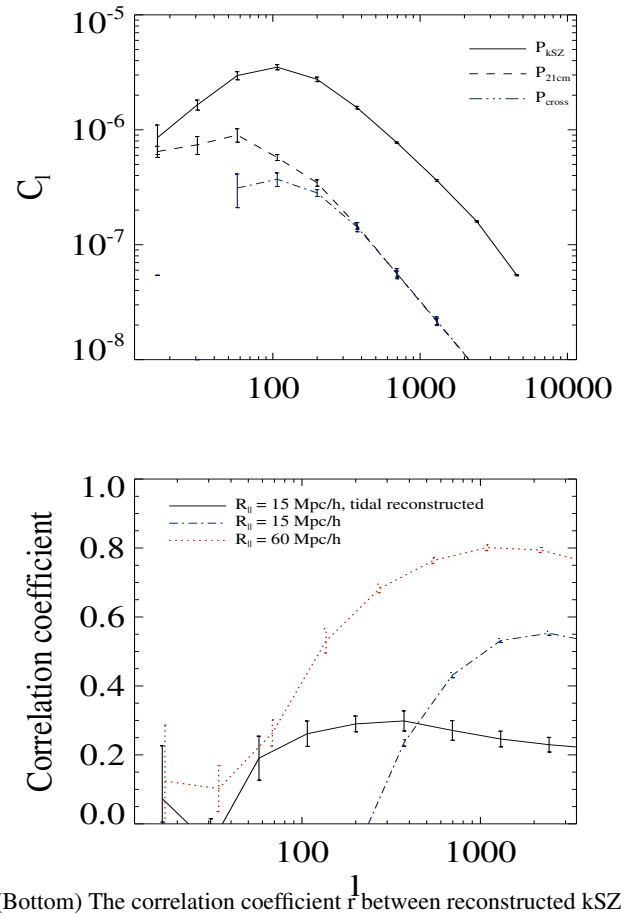

(Bottom) The correlation coefficient r between reconstructed kSZ signal and original kSZ signal.

FIG. 1: (Top)P_{kSZ}: powerspectrum of orginal kSZ signal Θ, P_{21cm}: powerspectrum of reconstructed kSZ signal from foreground substracted 21cm field with $R_{\parallel} = 15$ Mpc/h, after tidal reconstruction; P_{cross} the cross powerspectrum of this two fields;
(Bottom) The correlation coefficient r between reconstructed kSZ signal and original kSZ signal.

D. Simulation Results

We demonstrate the correlation effect of the reconstructed kSZ signal in Fig.II C. The upper panel shows the powerspectrum of orginal kSZ signal P_{kSZ}, reconstructed kSZ signal from 21cm intensity mapping P_{21cm} and the cross powerspectrum of this two field P_{cross}; and the lower panel demonstrates the correlation r between reconstructed kSZ signal $\hat{\Theta}$ and the orginal kSZ signal Θ. The results of correlation are shown in Fig.II C. The upper panel shows the powerspectrum of orginal kSZ signal P_{kSZ}, powerspectrum of reconstructed kSZ signal P_{21cm} from foreground substracted 21cm field with $R_{\parallel} = 15$ Mpc/h, after tidal reconstruction, and the cross powerspectrum of this two fields P_{cross}; The dark solid line in lower panel demonstrates the correlation r between original kSZ signal Θ and mock kSZ signal $\hat{\Theta}_{R_{\parallel}15,tide}$ from foreground substracted 21cm field with $R_{\parallel} = 15$ Mpc/h, after tidal reconstruction. As we can see, we have a stable 0.3 correlation

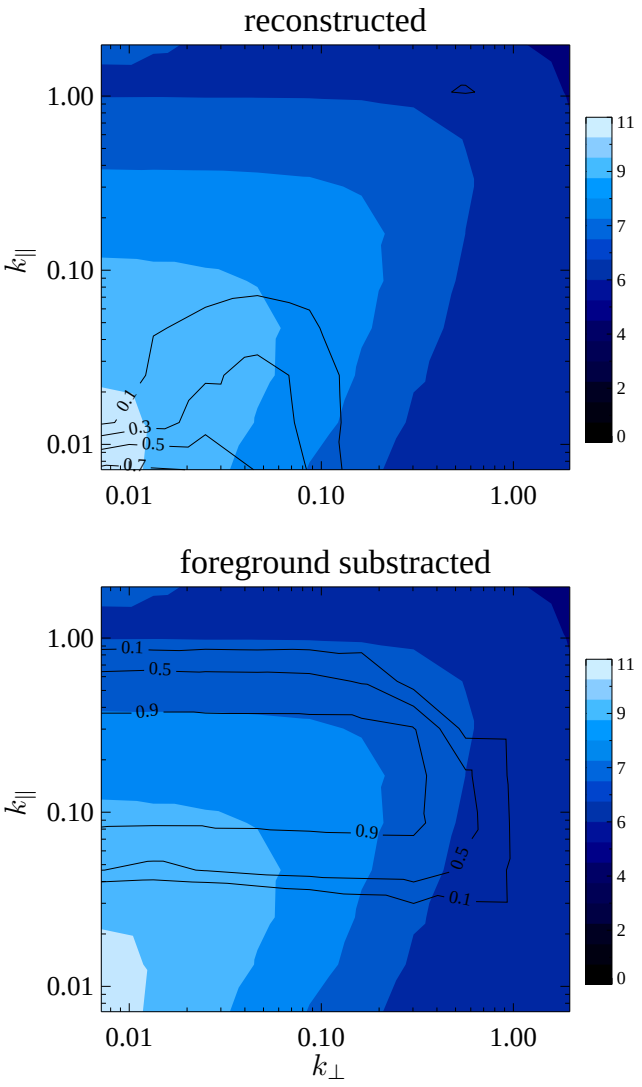

FIG. 2: (Top) Contour shows the correlation $r(k_\perp, k_\parallel)$ between the real velocity field v_z^{real} and $\hat{v}_z$ from the tidal reconstructed field; (Bottom) contour shows the correlation r between real velocity v_z^{real} and v_z^{fs} from the foreground substracted field. The background color indicating the level of powerspectrum of v_z^{real} in logrithm, $lg(P_{v_z^{real}})$

.

from $l \sim 100$ to $l \sim 2000$, which indicates a detectable signal in real observations.

III. WHY/WHEN TIDAL RECONSTRUCTION

One of the main concerns about employing Cosmic Tidal Reconstruction is that it will import additional noise. In this section, we will demonstrate that the newly recovered information on small $k_\parallel$ is far more important than the loss of accuracy on larger k modes in this problem, with typical foreground level, under current foreground substraction technology.

For comparison, we calculate the velocity field v_{fs} directly from the foreground substracted field δ_{fs} following identical procedure. In Fig.2, contours in upper panel show the correlation $r(k_\perp, k_\parallel)$ between the real velocity field v_z^{real} and foreground substracted velocity field v_z^{fs}; contours in lower panel show the correlation r between v_z^{real} and $\hat{v}_z$. The background color indicating the levels of velocity power spectrum $P_{v_z^{real}}$.

As we can see, although importing large noise to large k modes, the newly recovered small k_z modes contain information that corresponds to the highest level of P_v. These modes play a vital role in generating kSZ signals.

To better understand the behavior of kSZ signal, we write Eq.(6) in Fourier space.

$$\Theta(\boldsymbol{k}_\perp) \equiv \Theta(k_x, k_y, 0) = \int d^3k \delta(\boldsymbol{k}) v_z(\boldsymbol{k}_\perp - \boldsymbol{k}) \qquad (9)$$

Since $v(\boldsymbol{k}) \propto \delta(\boldsymbol{k})\frac{k_z}{k^2}$, its amplitudes drops much faster than $\delta(\boldsymbol{k})$ when k gets larger, therefore could be consider as delta function. So $\Theta(\boldsymbol{k}_\perp) \sim \delta(\boldsymbol{k}_\perp)$

When the foreground contaminate the small $k_\parallel$ modes, as seen from 2, we lose the original peak in $v(k)$ and hence select a totally different part of δ in mock kSZ signal.

From the blue dashed line in lower panel of Fig.II C, we can see the mock kSZ signal calculated directly from a typical foreground substracted fields($R_\parallel = 15$ Mpc/h) will not show any correlation with the real kSZ signal until ℓ gets greater than ~ 300.

On the other hand, aftering performing tidal reconstruction, we recover the modes with small k_z and tolerable $k_\perp$, which is close to the original peak in $v(k)$ and therefore enable us to get correlated signals.

However, we also have to noitice that by performing tidal reconstruction, we lost a portion of small $k_\parallel$ modes (reason discussed in [19]), which inhibits us from getting a better correlation.

If we consider a futuristic optimal case, when the foreground noise is low and removed quite successfully. Assume we have at least half density field structure remains at $k \sim 0.02$ Mpc/h, i.e. choose $R_\parallel = 60$ Mpc/h. Then we will be able to obtain a correlation of ~ 0.7 at $\ell \sim 300$ between the real kSZ sinal and mock kSZ signal directly from the original field, this is certainly better than using tidal reconstructed fields.

In all, the tidal reconstruction method is not designed to help us find the optimal correlation of the two signals, it is more like a safe belt that enable us to find a detectable correlation even when the measurement is not optimal. In the future, with telescope noises further supressed, better foreground substraction performed, we should obtain more accurate correlation results between kSZ signals and 21cm density field without any extra manipulations. However, with current and upcoming facilities, the signal will probably only be detected after tidal reconstruction. The algorithm greatly advances the time for us to cross correlate the two powerful probes—that is the value.

IV. STATISTICAL ERROR IN REAL SURVEYS

In real surveys, when we calculate the cross angular power spectrum C_l between reconstructed kSZ signals and CMB measurements, we will have to face statistical errors. They can be approximated as:

$$\frac{\Delta C_l}{C_l} \simeq \frac{1}{2rl\Delta l f_{sky}} \sqrt{\frac{C_l^{\rm CMB} + C_l^{ksz} + C_l^{{\rm CMB},N}}{C_{kSZ,\Delta z}(1+\frac{C^N_{\hat{\Theta}}}{C_{\hat{\Theta}}})}} \quad (10)$$

V. CONCLUSION AND FUTURE APPLICATION

VI. ACKNOWLEDGE

[1] R. J. Cooke, M. Pettini, R. A. Jorgenson, M. T. Murphy, and C. C. Steidel, ApJ **781**, 31 (2014), 1308.3240.

[2] G. Hinshaw, D. Larson, E. Komatsu, D. N. Spergel, C. L. Bennett, J. Dunkley, M. R. Nolta, M. Halpern, R. S. Hill, N. Odegard, et al., ApJS **208**, 19 (2013), 1212.5226.

[3] E. Komatsu, K. M. Smith, J. Dunkley, C. L. Bennett, B. Gold, G. Hinshaw, N. Jarosik, D. Larson, M. R. Nolta, L. Page, et al., ApJS **192**, 18 (2011), 1001.4538.

[4] G. Hinshaw, D. Larson, E. Komatsu, D. N. Spergel, C. L. Bennett, J. Dunkley, M. R. Nolta, M. Halpern, R. S. Hill, N. Odegard, et al., ApJS **208**, 19 (2013), 1212.5226.

[5] A. M. Sołtan, A&A **460**, 59 (2006), astro-ph/0604465.

[6] M. Fukugita and P. J. E. Peebles, ApJ **616**, 643 (2004), astro-ph/0406095.

[7] J. K. Werk, J. X. Prochaska, J. Tumlinson, M. S. Peeples, T. M. Tripp, A. J. Fox, N. Lehner, C. Thom, J. M. O'Meara, A. B. Ford, et al., ApJ **792**, 8 (2014), 1403.0947.

[8] R. Davé, B. D. Oppenheimer, N. Katz, J. A. Kollmeier, and D. H. Weinberg, MNRAS **408**, 2051 (2010), 1005.2421.

[9] R. A. Sunyaev and Y. B. Zeldovich, Comments on Astrophysics and Space Physics **4**, 173 (1972).

[10] R. A. Sunyaev and I. B. Zeldovich, MNRAS **190**, 413 (1980).

[11] N. Hand, G. E. Addison, E. Aubourg, N. Battaglia, E. S. Battistelli, D. Bizyaev, J. R. Bond, H. Brewington, J. Brinkmann, B. R. Brown, et al., Physical Review Letters **109**, 041101 (2012), 1203.4219.

[12] J. Shao, P. Zhang, W. Lin, Y. Jing, and J. Pan, MNRAS **413**, 628 (2011), 1004.1301.

[13] M. Li, R. E. Angulo, S. D. M. White, and J. Jasche, MNRAS **443**, 2311 (2014), 1404.0007.

[14] J. C. Hill, S. Ferraro, N. Battaglia, J. Liu, and D. N. Spergel, ArXiv e-prints (2016), 1603.01608.

[15] K. Bandura, G. E. Addison, M. Amiri, J. R. Bond, D. Campbell-Wilson, L. Connor, J.-F. Cliche, G. Davis, M. Deng, N. Denman, et al., in *Society of Photo-Optical Instrumentation Engineers (SPIE) Conference Series* (2014), vol. 9145 of *Society of Photo-Optical Instrumentation Engineers (SPIE) Conference Series*, p. 22, 1406.2288.

[16] Y. Xu, X. Wang, and X. Chen, ApJ **798**, 40 (2015), 1410.7794.

[17] http://www.acru.ukzn.ac.za/ hirax/.

[18] U.-L. Pen, R. Sheth, J. Harnois-Deraps, X. Chen, and Z. Li, ArXiv e-prints (2012), 1202.5804.

[19] H.-M. Zhu, U.-L. Pen, Y. Yu, X. Er, and X. Chen, ArXiv e-prints (2015), 1511.04680.

[20] T. Di Matteo, B. Ciardi, and F. Miniati, MNRAS **355**, 1053 (2004), astro-ph/0402322.

[21] K. W. Masui, E. R. Switzer, N. Banavar, K. Bandura, C. Blake, L.-M. Calin, T.-C. Chang, X. Chen, Y.-C. Li, Y.-W. Liao, et al., ApJ **763**, L20 (2013), 1208.0331.

[22] E. R. Switzer, T.-C. Chang, K. W. Masui, U.-L. Pen, and T. C. Voytek, ApJ **815**, 51 (2015), 1504.07527.

[23] J. Harnois-Déraps, U.-L. Pen, I. T. Iliev, H. Merz, J. D. Emberson, and V. Desjacques, MNRAS **436**, 540 (2013), 1208.5098.

[24] L. B. Newburgh, G. E. Addison, M. Amiri, K. Bandura, J. R. Bond, L. Connor, J.-F. Cliche, G. Davis, M. Deng, N. Denman, et al., in *Society of Photo-Optical Instrumentation Engineers (SPIE) Conference Series* (2014), vol. 9145 of *Society of Photo-Optical Instrumentation Engineers (SPIE) Conference Series*, p. 91454V, 1406.2267.

[25] X. Chen, International Journal of Modern Physics Conference Series **12**, 256 (2012), 1212.6278.

[26] K. W. Masui, E. R. Switzer, N. Banavar, K. Bandura, C. Blake, L.-M. Calin, T.-C. Chang, X. Chen, Y.-C. Li, Y.-W. Liao, et al., ApJ **763**, L20 (2013), 1208.0331.

[27] E. R. Switzer, K. W. Masui, K. Bandura, L.-M. Calin, T.-C. Chang, X.-L. Chen, Y.-C. Li, Y.-W. Liao, A. Natarajan, U.-L. Pen, et al., MNRAS **434**, L46 (2013), 1304.3712.